

# A Robust Open-source Tendon-driven Robot Arm for Learning Control of Dynamic Motions

Simon Guist<sup>1</sup>, Jan Schneider<sup>1</sup>, Hao Ma<sup>1</sup>, Vincent Berenz<sup>1</sup>, Julian Martus<sup>2</sup>, Felix Grüninger<sup>2</sup>, Michael Mühlebach<sup>1</sup>, Jonathan Fiene<sup>2</sup>, Bernhard Schölkopf<sup>1</sup> and Dieter Buechler<sup>1</sup>

**Abstract**—A long-lasting goal of robotics research is to operate robots safely, while achieving high performance which often involves fast motions. Traditional motor-driven systems frequently struggle to balance these competing demands. Addressing this trade-off is crucial for advancing fields such as manufacturing and healthcare, where seamless collaboration between robots and humans is essential. We introduce a four degree-of-freedom (DoF) tendon-driven robot arm, powered by pneumatic artificial muscles (PAMs), to tackle this challenge. Our new design features low friction, passive compliance, and inherent impact resilience, enabling rapid, precise, high-force, and safe interactions during dynamic tasks. In addition to fostering safer human-robot collaboration, the inherent safety properties are particularly beneficial for reinforcement learning, where the robot’s ability to explore dynamic motions without causing self-damage is crucial. We validate our robotic arm through various experiments, including long-term dynamic motions, impact resilience tests, and assessments of its ease of control. On a challenging dynamic table tennis task, we further demonstrate our robot’s capabilities in rapid and precise movements. By showcasing our new design’s potential, we aim to inspire further research on robotic systems that balance high performance and safety in diverse tasks. Our open-source hardware design, software, and a large dataset of diverse robot motions can be found at [webdav.tuebingen.mpg.de/pamy2/](http://webdav.tuebingen.mpg.de/pamy2/).

## I. INTRODUCTION

Human arm movements encompass a broad array of distinct motion characteristics, including slow and precise motions for object manipulation, high-force trajectories for carrying heavy objects, and fast movements for dynamic tasks, such as sports games. Replicating the full range of these capabilities, along with the inherent safety properties of human arm movements, such as compliance and backdrivability, has been a challenging endeavor in robotics research.

A key enabling factor to approach this performance is allowing robotic systems to establish more contacts with their environment than currently possible with conventional rigid systems. Contacts can reduce the task’s uncertainty mechanically by constraining dimensions in the state space, such as positions or velocities, as famously described in Mason’s funnel metaphor [1]. For instance, writing with a pen becomes significantly more precise when the elbow rests on the table, in contrast to moving freely. The fixed point at the elbow reduces the variability at the tip of the pen. Additionally, extending the set of allowed contacts enables the control algorithm to be less conservative and take more risks to optimize for performance. In that manner, robots could move at higher speeds if the

negative consequences of unintended impacts are reduced. Moving at higher speeds enables the robot to solve tasks quicker, but damage to the robot and the environment is more likely.

Success in robotics is often measured by how well robots perform in human-created environments and tasks such as working alongside humans and integrating seamlessly, or doing housework like cleaning kitchens without breaking any items. These settings have not been built for robots but for humans who excel in safe contacts. Attempting to perform the same contacts in such tasks with current rigid robots would possibly lead to failure for even slight environmental changes.

For motor-driven rigid robots, collision avoidance often necessitates the use of 1) environmental sensors and tracking systems, 2) limiting the robot’s speed or 3) range of motions. Still, these techniques may not prevent all collisions while constraining the robot’s performance. For this reason, collaborative robots or “cobots” have been invented. These robots are relatively slow and weak but safe for human interaction compared to industrial robots that are fast and precise but prone to damage upon collision. With rigid and motor-driven systems, a trade-off seems to exist between speed and precision on one hand and safety on the other.

Alternatively, the negative effects of collisions could be significantly reduced by using soft robots. These systems often rely on stretchable components as well as compressible fluids. Continuous scratching along the surfaces of such materials can lead to damage since soft robots are generally less durable compared to rigid robots. Also, accurate control of fully soft robots, such as Baymax [2], tends to be problematic.

Ideally, robotic hardware would support the algorithm to execute motions that are (i) fast, (ii) precise, (iii) capable of generating high forces when necessary, and (iv) inherently minimize the probability of impact and its potential damage. While rigid motor-driven robots cover (i) to (iii), soft robots fulfill (i), (iii), and (iv).

We strive to accomplish all four desired motion capabilities by adapting the mechanical design of the robot. In particular, we base our design on the insights that accuracy requires rigid parts while impact resilience implies low force transmission. Aside from velocity, the primary factors influencing impact forces are the robot’s inertia and rigidity [3, 4].

Rigidity and inertia can be significantly reduced by pairing soft actuation, such as pneumatic artificial muscles (PAM), with tendon drives. PAMs offer the advantage of avoiding stiff joints, which results in less severe peak forces when collisions occur. At the same time, this type of actuator can generate great forces to achieve either fast motions or lift heavy objects.

<sup>1</sup>Max Planck Institute for Intelligent Systems, 72076 Tübingen, Germany. [firstname.lastname@tuebingen.mpg.de](mailto:firstname.lastname@tuebingen.mpg.de)

<sup>2</sup>Max Planck Institute for Intelligent Systems, 70569 Stuttgart, Germany. [lastname@is.mpg.de](mailto:lastname@is.mpg.de)

Tendon drives allow building robot arms with minimal moving masses by transferring the actuation to the robot base. Such robot designs can be safe, even when operating at increased velocities, due to their inherent backdrivability and low inertia. However, precise control is an issue. The main problem is that the high-force transmission through tendon drives wears out the tendon guidance, and high amounts of friction typically add non-linearities and stochasticity. Also, PAMs are nonlinear actuators that change their dynamics with temperature and exhibit hysteresis effects.

In this work, we present a durable and fast 4-DoF tendon-driven robot arm with significantly lower friction than previous designs. The powerful actuators, low inertia, and backdrivability ensure that our design satisfies conditions (i), (iii), and (iv). Furthermore, due to its low friction, our robot outperforms previous tendon-driven robots in condition (ii). We thoroughly evaluate each of these claims. To that end, we show that our system is more linear than the previous design [5, 6], highlight the lower friction of our new tendon guidance, perform a repeatability test, let the robot run for 25 days uninterrupted, and perform impact experiments, illustrating that our system produces similar impact forces to the Franka Panda and UR5e at  $\sim 4\times$  the speed. Ultimately, we learn table tennis smashes with reinforcement learning (RL) as in [7] and double the ball’s speed while simultaneously improving precision. The setting is identical down to the hyperparameters, showing that just by using the new robot, performance substantially improved.

To accelerate progress on learning for dynamic tasks, we open-source the design as well as the entire software infrastructure required to run our system, including a C++ and Python interface. Since our system uses mainly off-the-shelf, commercially available components, 3D-printed parts, and only few custom-machined parts, practitioners are welcome to modify the design and customize our system to their needs.

The main contribution of this work is the design of a robot arm (i) that is less prone to damage upon collision due to its lightweight construction, passively compliant actuation, and tendon drives, (ii) with enhanced ease of control, achieved by minimizing non-linearities, primarily caused by high friction, (iii) that allows for repeatable dynamic motions facilitating the collection of large amounts of data for long-term training, (iv) designed for replicability and adaptability, which allows researchers to build upon and customize our work for their specific research question.

In Section III, we present the key design decisions that accomplish these objectives. These include a description of the tendon-driven design and the choices that allowed us to reduce friction in the cables and joints, and to increase the system’s robustness. In Section IV, we conduct experiments to demonstrate our system’s effectiveness. We perform long-term dynamic motions to verify robustness and conduct measurements to quantify impact safety. To showcase enhanced ease of control, we demonstrate the increased linearity of our robot in comparison to the previous system. Finally, we apply our system to a challenging dynamic table tennis task, illustrating its capacity for rapid and precise movements.

## II. RELATED WORK

Safety in robotics is typically tackled by instrumenting the environment with sensors to detect and track humans and obstacles in the workspace. Sensors employed for this purpose range from distance sensors mounted to the robot [8] to depth cameras [9] and marker-based motion capture systems [10]. If the distance between the robot and a human or obstacle is below a threshold, a safety controller adapts the robot motion to avoid a collision [9] or slows down and stops the motion [10, 11]. These methods generally come with additional costs for the sensors and the need for sensor calibration. Due to the potential for occlusions, they typically require multiple sensors that capture the scene from different angles. Furthermore, collision avoidance strategies tend to be very conservative because they aim to avoid collisions at all cost, resulting in a robot that is heavily constrained in its motions.

Robot safety is particularly important when training policies via RL. During training, the RL agent typically explores random actions. Due to the uncontrolled nature of these exploration strategies, the resulting motions can be dangerous for both the robot and its environment. Safe RL aims to mitigate these safety concerns by discouraging the agent from visiting unsafe states. To that end, these methods modify, e.g., the optimization objective [12, 13, 14, 15], the exploration behavior [16, 17, 18, 19], or the action selected by the policy [20, 21, 22]. Unless provided with additional domain knowledge, safe RL methods need to explore dangerous states at least once during training to learn that these states are unsafe [23]. Domain knowledge, e.g., in the form of a dynamics model or an expert policy, might not always be available, and visiting an unsafe state even once can already cause severe damage to the robot or its environment.

Inherently compliant robots are a viable option to alleviate some safety requirements and avoid the extensive use of sensors for collision avoidance and the dependence on domain knowledge for safe RL. Soft robot components, like passively compliant joints [24] or links [25], can significantly reduce contact forces upon collision. Gealy et al. [26] built a 7-DoF robot arm that achieves passive compliance through backdrivable transmissions. GummiArm [27, 28] and BioRob [29] employ elastic tendons for mechanical compliance. An alternative is offered by PAMs, which are inherently compliant actuators that can achieve high forces. These actuators are widely used in human-inspired robot arms [30, 31, 32, 33, 34]. Passively compliant robots can also be combined with active collision avoidance strategies, such as in [35]. In such a combination, the robot’s compliance enhances safety in the event of undetected or unavoidable collisions.

Safety through compliance is essential in dynamic tasks because collisions are more likely at high velocities, and impacts are more severe due to the high momentum of the robot. However, fast motions apply additional strain to the system and, therefore, few robot designs in the literature are capable of generating dynamic motions. Stoelen et al. [27] demonstrate fast ballistic movements with the GummiArm. Ikemoto et al. [33] evaluate their design on a dynamic throwing

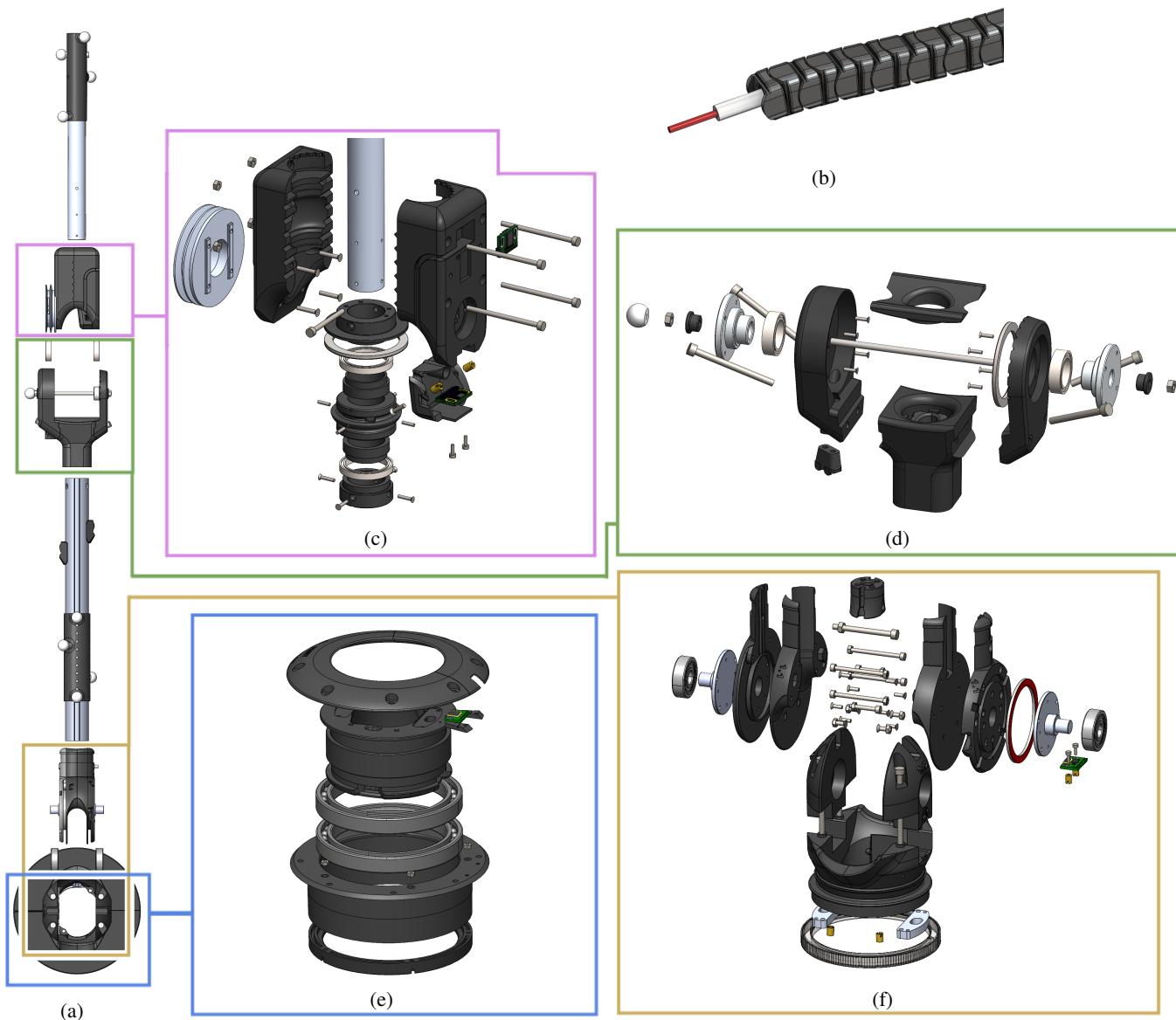


Fig. 1: Design of the new tendon-driven robot arm (a). The arm has a rotational and a swivel DoF within the first (e), (f) and second joint (c), (d). It features ball bearings, which are low in friction. Many parts are self-designed and 3D-printed, which are shown colored in black. The four angle encoders are shown with a small green circuit board. The Bowden tubes (b) feature an inner tube and outer support elements that help maintain constant tendon length.

task. The BioRob arm [29] is able to achieve end effector velocities of 7.4 m/s [36]. Mori et al. [37] designed a high-speed robot for a highly dynamic badminton task, which achieves racket speeds of 21 m/s. However, none of these robots were evaluated in long-term experiments, so it remains unclear whether these dynamic motions can be executed robustly over long time periods.

### III. REALIZATION OF PAMY2

In this section, we present the design of our robot, PAMY2, which substantially advances the design of the prior tendon-driven robot introduced by Büchler et al. [5], referred to as PAMY1 throughout the paper. We detail the improvements made to the mechanical design, Bowden tubes, bearings, and pneumatics. Furthermore, we discuss our design choices in

light of the goals of impact safety, robustness, and ease of control. The mechanical design of the arm is depicted in Figure 1.

#### A. Design Choices to Improve Impact Safety

Because collisions cannot always be avoided without limiting the performance of the robot, one of the primary design objectives is to ensure that the impact of such collisions is limited. We achieve this goal by incorporating a tendon-driven design and using passively compliant actuators. As can be seen in Figure 1, the actuators of our robot are not on the robot arm but on the base. Therefore the moving masses (about 1.3 kg) and inertia are small compared to traditional robot designs where actuators are typically located at the joints.

Active and passive compliance are two distinct approaches to achieving compliance. Active compliance utilizes sensor data and feedback control to adapt and respond to external forces. One example of active compliance are collision reaction schemes. However, the reaction times are often too long to prevent damage. In contrast, passive compliance is achieved through the inherent mechanical properties of the robot, such as elastic joints or soft materials. Our robot achieves passive compliance through the use of PAM actuators. These actuators are inherently compliant, allowing the robot to absorb and dissipate external forces without the need for complex control schemes.

### B. Design Choices to Increase Ease of Control and Extend Durability

Reducing friction is essential for improving the robot’s ease of control, as it reduces uncertainties and nonlinearities in the dynamics. Furthermore, friction leads to wear, which limits the system’s longevity. This section highlights the design choices that help minimize friction in our robot.

1) *Bowden Tubes*: Improving the Bowden tubes is key to addressing friction, durability, and maintenance challenges commonly encountered in tendon-driven systems. Our design incorporates continuous Polytetrafluoroethylene (PTFE) Bowden tubes. Using PTFE significantly reduces friction and heat generation, prolonging tendon lifespan. Furthermore, these tubes exhibit resistance to kinking and separation, effectively minimizing the risk of tendon entanglement. In addition, our system features a design consisting of an inner tube and custom outer support elements, as depicted in Figure 1b. These outer support elements were specifically engineered for easy 3D printing. This novel design ensures a constant tendon length during arm movements by providing external support. Consequently, the movement of different joints is effectively decoupled, improving overall system precision.

In our design, we employ a knot-based tendon attachment method, circumventing the drawbacks of adhesive-based attachments, such as long drying times, limited shelf life, and decreased bonding strength. Various knot types have been extensively tested for durability across different material thicknesses. Moreover, the end connections to the muscles are designed to enable easy length adjustments and maximize force transmission, avoiding force reduction due to unfavorable knots or adhesive bonding.

2) *Bearings*: The previous design utilized gliding bearings, which offered the benefit of being highly compact. However, they exhibit substantial friction and stiction. In contrast, our updated design features ball bearings as a replacement. This new design results in a substantial reduction in friction and stiction.

### C. Improved Pneumatics

In the pneumatic system of our tendon-driven robot arm, we have implemented several optimizations to enhance performance and reliability. First, we employed optimized tube routing to improve airflow and reduce pressure losses, particularly by avoiding sharp 90-degree angles in the pneumatic lines.



Fig. 2: Experimental setup for the collision force measurements. A Pilz PRMS is mounted to a table onto which the end effector of the robot is colliding.

Second, we incorporated a buffer reservoir to stabilize the air pressure supply in front of the valves, ensuring consistent and efficient actuation. Lastly, we designed a ring circuit for the pneumatic system, further improving the air pressure distribution among the valves.

### D. Open-Source Hardware and Software

To facilitate further research and development in dynamic robotic tasks, we have made both the hardware and software components of our robot open-source.

1) *Hardware*: Our approach aims at enabling others to build upon our work and adapt the robot for specific applications. The design primarily employs off-the-shelf, commercially available components, 3D-printed parts, and only a limited number of custom-machined parts, thus making it cheaper than many other industrial or research robots. It is important to note, however, that for the 3D-printed components, specialized printers, such as those from the company Markforged or comparable alternatives, capable of reinforcing parts with continuous fibers, are required.

2) *Software*: We provide an open-source software framework with a versatile API in Python and C++ for controlling and monitoring the robot, based on the o80 framework [38]. The o80 software framework interfaces with the robot’s Programmable Logic Controller (PLC). Communication between the PLC and the o80 software running on the PC is facilitated through UDP, transmitting data such as the robot state (joint angles and velocities, muscle pressures, and valve positions), actions (target pressures or target positions, depending on the control mode), and error information.

## IV. EXPERIMENTS & EVALUATIONS

In this section, we present a series of experiments designed to assess the efficacy of our new robot arm. Our experiments focus on evaluating the following characteristics: impact safety, robustness, ease of control, and the ability to perform rapid and precise movements.

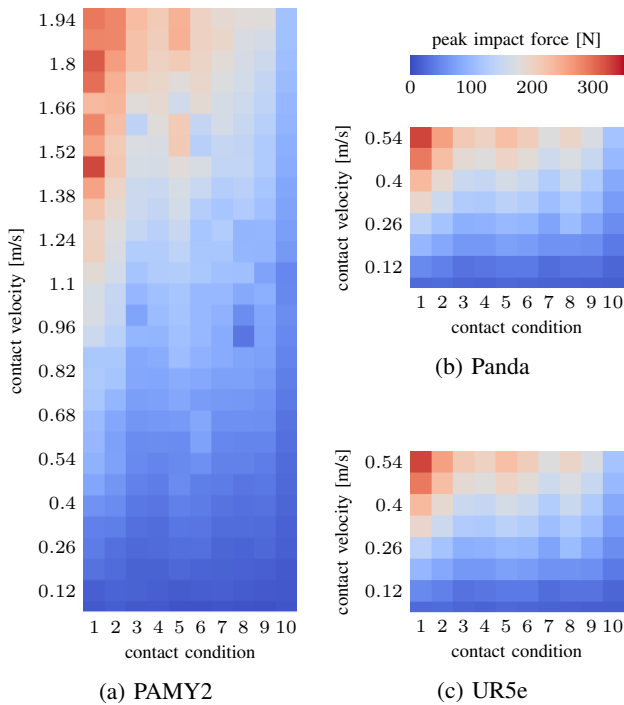


Fig. 3: Collision force map depicting peak impact forces resulting from varying impact velocities and contact scenarios for our robot, alongside the Franka Emika Panda and the Universal Robot UR5e for comparison. Our findings reveal that our robot, when operating at high velocities, generates impact forces akin to those exhibited by the other two robots at considerably lower velocities. We express our gratitude to Kirschner et al. [39] for generously sharing the impact data for the Panda and UR5e robot arms.

#### A. Evaluating Impact Safety

One of the main goals of our tendon-driven robot arm is to ensure superior impact safety compared to traditional motor-driven systems. We achieve this objective primarily through the tendon-driven design, which relocates the heavy actuators to the robot base. Although the use of compliant actuators contributes to the overall safety of the robot, the system’s inertia primarily determines the peak force at impact.

To evaluate the impact safety of our robot, we examine the peak force occurring during potential collisions. For our experiments, we employ the Pilz Robot Measurement System (PRMS) to measure forces during collisions. This device comprises a one-dimensional load cell, a spring, and a rubber cover. Various springs and covers are available to adjust the stiffness according to different human body parts based on ISO/TS 15066:2016 specifications [40], as shown in Table I. This technical specification introduces a model of the human body, covering 21 body regions. For each body region, it provides a contact stiffness and a pain tolerance.

We compare our measurements to the results obtained in previous studies by Kirschner et al. [4, 39]. To ensure that our measurements accurately reflect the impact safety of our robot, we measure the forces at a position close to the robot center. This position ensures that most of the robot’s mass contributes

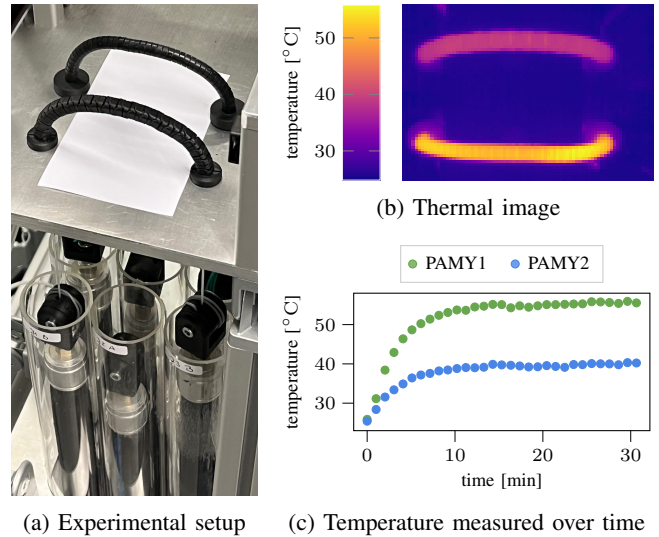


Fig. 4: Experiment comparing the friction of our Bowden tubes (top) with those utilized by [5] (bottom). The experimental setup is illustrated in (a): Both types of Bowden tubes are actuated by rapid-switching muscles of the same type. The thermal camera’s heat map (b) and the temperature evolution over time (c) both show a significantly lower temperature increase for our Bowden tubes. This indicates a substantial reduction in friction.

to the peak force experienced during a collision. Figure 2 illustrates the robot’s position during the measurements. To collect the data, we execute trajectories with linear changes in muscle pressure. Upon detecting a sudden change in velocity, indicating a potential collision, we halt the movement by keeping the target pressure fixed. By modifying the rate of change of the target pressure, we evaluate the impact safety of our robot at various velocities.

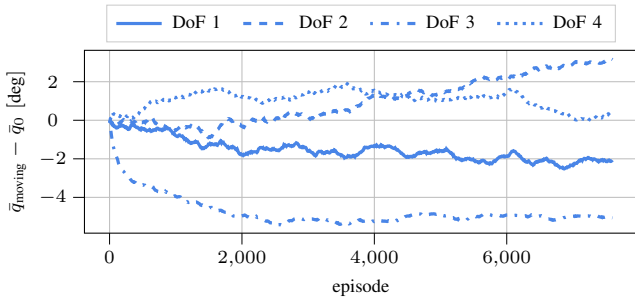
The data depicted in Figure 3 shows peak forces during collisions for our tendon-driven arm and for the Franka Emika Panda and Universal Robots UR5e, two conventional motor-driven systems, investigated in prior research. The results clearly show the superior impact safety of our robot, as it achieves similar contact forces while moving at almost four times the speed of traditional motor-driven systems.

However, it is important to emphasize that although our tendon-driven arm is significantly safer compared to other robotic arms, it could still cause serious injuries if a human is struck with full force at high speeds. Future work should focus on further enhancing the safety of our system by combining its inherently safer hardware design with algorithmic approaches, additional sensors, or safety mechanisms.

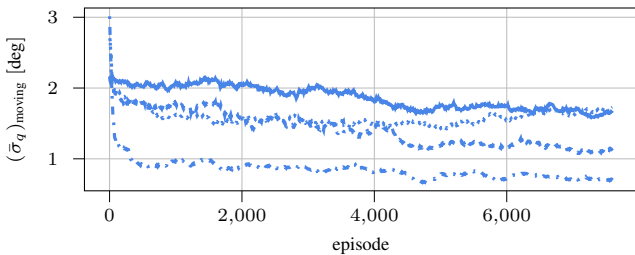
#### B. Evaluating Robustness

Reinforcement learning enables robots to achieve high performance in complex tasks. However, for these approaches, training for long durations is crucial. We aim to produce a system that lasts and is reliable and therefore minimize the main contributor to failure: friction.

1) *Friction Quantification*: Friction plays a significant role in tendon-driven robots as it converts kinetic energy into



(a) Mean of the final position



(b) Standard deviation of the final position

Fig. 5: Moving mean position relative to the initial mean position  $\bar{q}_{\text{moving}} - \bar{q}_0$  and the standard deviation  $(\bar{\sigma}_q)_{\text{moving}}$  of the robot’s final position after the open-loop reset motion during the approximately 25 days of the long-term experiment. It uses a moving average window of 400 episodes. A stable mean position (a) alongside a small and slightly decreasing standard deviation (b) over time indicates consistent performance throughout the long-term experiment.

thermal energy. Because it is widely acknowledged that using ball bearings instead of sliding contact bearings is an effective way to reduce friction, we focus our experiments on evaluating the other major source of friction in our tendon-driven robot, the Bowden tubes.

To assess this friction and compare it with the original system from [5], we utilize a thermal camera to measure the heat generated during operation. We set up an experiment where two muscles are connected directly using a Bowden tube, as shown in Figure 4a. The antagonistic muscle pair is contracted in an alternating manner at a frequency of 3.33 Hz for 30 minutes. Figure 4b displays the thermal image captured at the end of the experiment, which indicates that our Bowden

tube remained substantially cooler than the original. A more detailed analysis of the temperature change in the two Bowden tubes can be seen in Figure 4c. The data points in the plot represent the median temperature of the five hottest pixels in the corresponding Bowden tube’s image region. The graph illustrates that the temperature of the original tubes rises more rapidly and ultimately converges to a higher value. These measurements confirm that the design of our Bowden tubes offers significantly lower friction than the original system.

2) *Long-term Dynamic Motions*: Learning complex skills with real robots often necessitates numerous interactions with the environment. To showcase our robot’s capability in collecting the data required for mastering dynamic tasks, we conduct a long-term experiment involving various dynamic movements. This experiment evaluates the system’s reliability and robustness over extended periods.

We designed an array of movement patterns, encompassing random multisine signals, fixed target pressure movements with varying time intervals, and reset motions. The reset motion, executed in an open-loop fashion without feedback from angle position measurements, involves moving to medium pressures, then to minimum pressures, and finally to medium pressures again. This particular reset motion was chosen to make the final position more independent of the preceding position or motion, thus making differences in this position more indicative of changes in hardware.

During the experiments, the robot operated continuously for approximately 25 days, amassing a comprehensive dataset of diverse robotic motions. The data was recorded at a high sampling rate of 500 Hz. The dataset includes the current and desired pressure for each muscle, the position and velocity of each joint, as well as timestamps.

Throughout the long-term experiments, the robot exhibited a high level of robustness and reliability, with no significant signs of wear or damage. This outcome underscores the effectiveness of our design in ensuring the robot’s durability during dynamic tasks.

To quantitatively assess the system’s repeatability, we analyzed the robot’s final position after executing the reset motion multiple times. The small deviation in the final positions, illustrated in Figure 5, indicates that the system maintains consistent performance even after prolonged usage. This repeatability is crucial for successful reinforcement learning, as it ensures the robot can reliably execute learned policies.

TABLE I: Definition of contact conditions based on ISO/TS 15066 [40].

No.	Body part	Stiffness	Hardness	Pain Threshold
1	Skull	150 N/mm	70 ShA	130 N
2	Face/hand	75 N/mm	70 ShA	65 N
3	Lower legs	60 N/mm	30 ShA	260 N
4	Thighs	50 N/mm	30 ShA	300 N
5	Neck	50 N/mm	70 ShA	440 N
6	Lower arms	40 N/mm	70 ShA	320 N
7	Back	35 N/mm	30 ShA	420 N
8	Upper arms	30 N/mm	30 ShA	300 N
9	Chest	25 N/mm	70 ShA	280 N
10	Abdomen	10 N/mm	10 ShA	220 N

### C. Evaluating Ease of Control

1) *Increased Linearity*: We employ the method proposed by Ma et al. [41] for system identification in the frequency domain to quantify the nonlinearity in PAMY1 and PAMY2. Each degree of freedom is treated as a single-input and single-output (SISO) system. We design ten different excitation signals with the same frequency spectrum and ten randomly chosen phase spectra, exciting the frequency lines  $\Omega = \{0.1\text{Hz}, 0.2\text{Hz}, \dots, 10\text{Hz}\}$ .

We excite each degree of freedom individually. Each excitation signal is applied for ten periods continuously, and the response signals of the first two periods are discarded

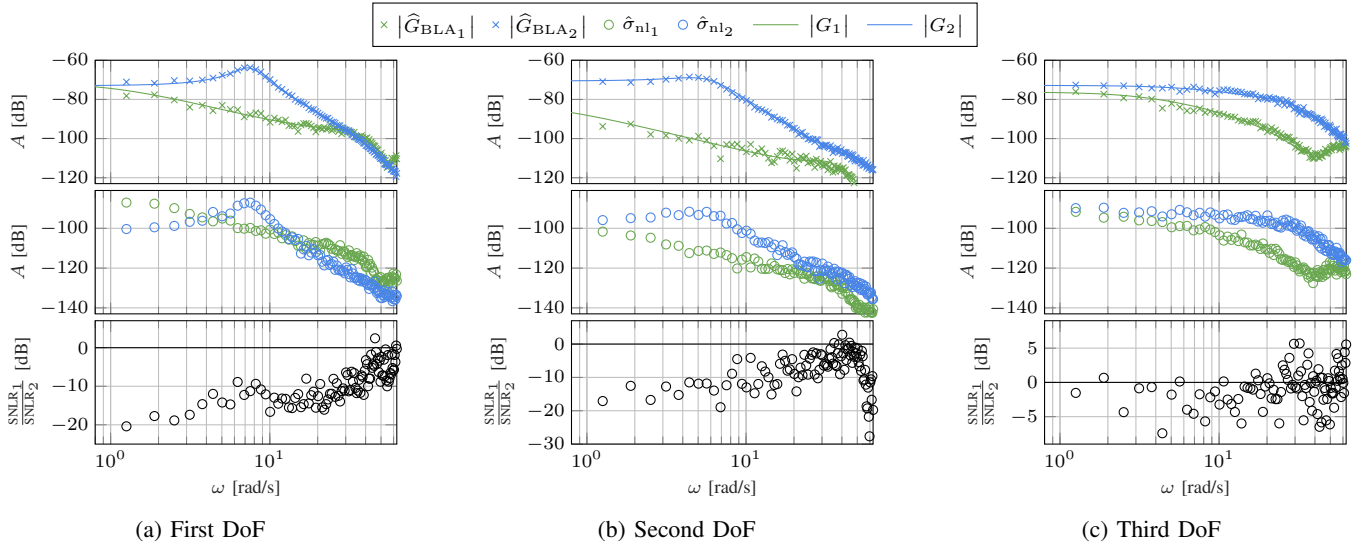


Fig. 6: Comparison of the linearity between PAMY1 (index 1) and PAMY2 (index 2). The new system demonstrates increased amplitude ( $A$ ) and a higher bandwidth across all DoFs (first row). The second row shows the absolute level of nonlinearity of the two systems. To make this nonlinearity between the systems comparable, we examine the SNLR (third row), which is significantly lower for the first two DoFs at most frequencies, and marginally lower for the third DoF at lower frequencies. These findings underscore the enhanced tracking performance and reduced nonlinearity of the new system.

to avoid the effect of transients. Let  $U^i(j\omega_k)$  and  $Y^i(j\omega_k)$  with  $i = 1, \dots, p$  and  $\omega_k \in \Omega$  denote the discrete Fourier transformation (DFT) of the input (difference in target pressure for antagonistic muscle pairs) and output signals (joint angles) of the  $i$ -th period, respectively, where  $p$  represents the total number of periods after discarding (here  $p = 8$ ), and  $j = \sqrt{-1}$  denotes the imaginary number. First of all, we calculate the average value of the input and output signals in the frequency domain over all the different periods.

$$\hat{Y}(j\omega_k) = \frac{1}{p} \sum_{i=1}^p Y^i(j\omega_k) \quad (1)$$

$$\hat{U}(j\omega_k) = \frac{1}{p} \sum_{i=1}^p U^i(j\omega_k) \quad (2)$$

The average frequency response function (FRF)  $\hat{G}$  is given by

$$\hat{G}(j\omega_k) = \frac{\hat{Y}(j\omega_k)}{\hat{U}(j\omega_k)}. \quad (3)$$

Since the identified system is nonlinear, the discrepancy between the measured average FRFs that arise when having excitation signals with different phase spectra provides a means to characterize the nonlinearities. If the system were linear, then applying excitation signals with different phase realizations would not affect the average FRF. First, we calculate the corresponding average FRF  $\hat{G}^l$ ,  $l = 1, \dots, m$  for each input signal according to Equation (3), where the superscript  $l$  refers to the different excitation signals (here  $m = 10$ ). Then, the average FRF over all excitation signals is given by

$$\hat{G}_{\text{BLA}}(j\omega_k) = \frac{1}{m} \sum_{l=1}^m \hat{G}^l(j\omega_k), \quad (4)$$

where the subscript BLA refers to “Best Linear Approximation”. Lastly, an estimate of the system’s nonlinearity is given by

$$\hat{\sigma}_{\text{nl}}^2(j\omega_k) = \frac{1}{m(m-1)} \sum_{l=1}^m \left| \hat{G}^l(j\omega_k) - \hat{G}_{\text{BLA}}(j\omega_k) \right|^2, \quad (5)$$

where the subscript nl refers to “nonlinearity”.

The system identification results are shown in Figure 6. We observe that the new system exhibits higher amplitudes compared to the old system, indicating improved tracking of dynamic and fast motions. At the same time, each system’s degree of nonlinearity and amplitude show the same trend. To better compare the degree of nonlinearity of the two systems, we define the signal-to-nonlinearity ratio (SNLR) as

$$\text{SNLR}(j\omega_k) = \left( \frac{|\hat{G}_{\text{BLA}}(j\omega_k)|}{\hat{\sigma}_{\text{nl}}} \right)^2. \quad (6)$$

We note that the absolute value of  $\hat{\sigma}_{\text{nl}}^2$  is not a good indicator since it would be affected by a simple re-scaling of the output variable.

The third row in Figure 6 shows the ratio of the SNLR for the two systems. We notice that in a large portion of the frequency spectrum, the SNLR value of the old system is significantly smaller than that of the new system, especially for the first and second DoF. When adjusted for amplitude, this result shows that the new system has significantly lower nonlinearity than the old system. This indicates that the new system will be easier to control, which we will demonstrate in the next experiment.

2) *Learning a Dynamic Task*: To demonstrate our system’s capabilities in a highly dynamic task, we repeat the table tennis

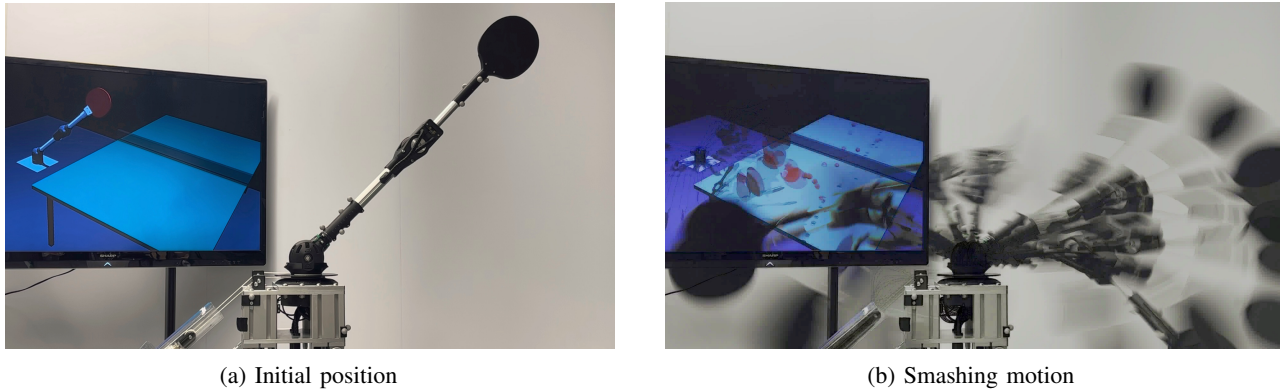


Fig. 7: Table tennis smashing experiment with PAMY2. In the HySR setup, we learn with a real robot and a simulated ball. The robot’s initial position at the beginning of an episode is shown in (a). During the training, the robot learns a motion in which it first draws back to generate momentum before striking the ball (b). The racket reaches speeds of up to 12 m/s during this motion.

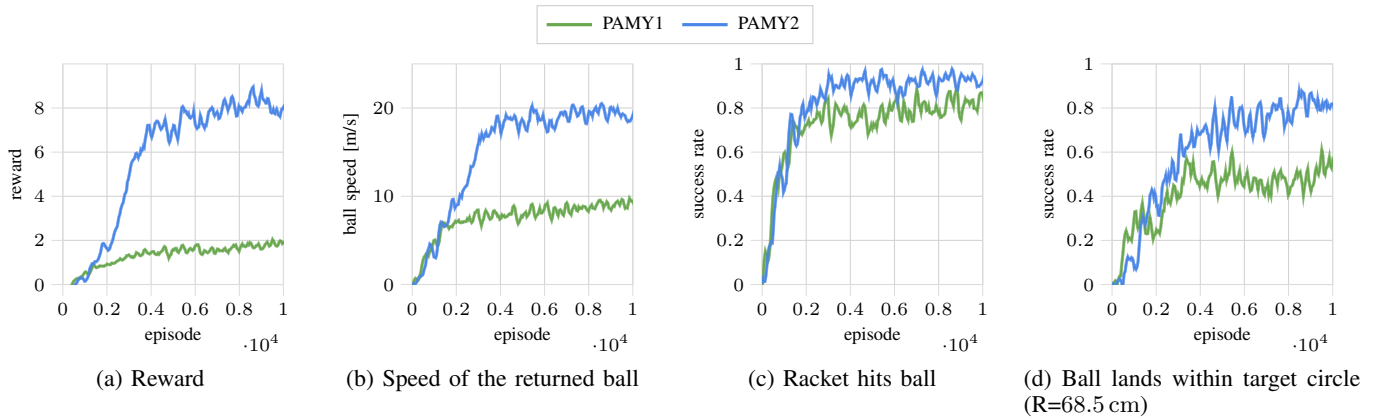


Fig. 8: Results of the table tennis smashing experiment. Compared to the old design, PAMY2 reaches a significantly higher final reward (a). Analyzing this result in detail, we find that it returns balls with higher average speed (b), but at the same time also hits the ball more often (c), and more often the ball lands close to the target position (d). This experiment demonstrates the benefits of the new design for motions that are highly dynamic but also precise.

smashing experiment from [7]. This task employs a reward function that includes both the ball’s speed and accuracy with respect to a target location on the other side of the table. It is a good demonstration of the robot’s potential, as it requires rapid and precise movements, as well as high forces to accelerate the ball to high velocities. Similar to Büchler et al. [7], we train the robot in a Hybrid-Sim-and-Real setup (HySR), with the real robot and a simulated ball as shown in Figure 7. Büchler et al. [7] show that the robot can return real balls, albeit training only with simulated balls.

We use a stochastic policy, with actions being changes in target pressures, and use Proximal Policy Optimization (PPO) [42] as the backbone RL algorithm. Although there were changes in the software, we aimed to keep the setup as similar as possible to [7] to allow for a direct performance comparison. It is worth noting that the learning hyperparameters were optimized for the old system, and we decided not to adapt or optimize them further for our new system to ensure that any performance gains are caused by hardware improvements, not by hyperparameter changes.

As a result of the increased activation bandwidth and also

due to the robot discovering an effective strategy of moving along the joint limit of the second DoF before striking the ball, we found that the learning algorithm frequently pushed the robot towards its joint limits, which is detrimental to the robot’s longevity. To address this issue and minimize wear and tear on the robot, we introduced a minor term to the reward function that discourages reaching the joint limits. Crucially, aside from this adjustment, no further safety measures are necessary, underscoring the inherent robustness of the PAMY2 design.

Figure 8 shows that the new design, PAMY2, achieves significantly higher ball speeds than the previous design. Despite the higher ball speeds, it is also more precise in terms of more frequent ball contacts and lower distance to the ball’s target location. Overall, PAMY2 reaches performance far superior to PAMY1, demonstrating the benefits of the improved design for highly dynamic and precise motions.

## V. DISCUSSION AND CONCLUSION

In this paper, we have presented a novel 4-DoF tendon-driven robot arm actuated by PAMs. Our design focuses on

reducing friction, passive compliance, and inherent impact safety, allowing the robot to operate efficiently and safely during dynamic tasks. Through various experiments, we have demonstrated the effectiveness of our robotic arm in terms of these design goals.

Our work contributes to the growing field of soft robotics, which aims to create more adaptable and safer robots, particularly for human-robot interaction scenarios. Although our robot arm showcases several advantages over traditional motor-driven systems, there are limitations to our design. Despite the improvements in terms of ease of control, PAM-driven systems still face challenges in achieving the repeatability and precision offered by their motor-driven counterparts. Identifying the optimal set of tasks for our robot arm, where the benefits of safety and dynamic performance outweigh the limitations, is an important avenue for future research. Recent advances in machine learning for robotics hold great opportunities for enhancing the capabilities of robots like ours. In the table tennis task, we showed that with our improved design, and by leveraging data-driven approaches, it is possible to develop advanced control strategies that address the inherent challenges of PAM-driven systems.

Our work represents a step forward in the development of robotic systems that can achieve high performance while maintaining safety in shared human environments. By making our design and resources open-source, we hope to inspire future research efforts that build upon and refine our work, fostering a new generation of collaborative and versatile robots.

#### REFERENCES

- [1] M. Mason, "The mechanics of manipulation," in *1985 IEEE International Conference on Robotics and Automation*, vol. 2. IEEE, 1985, pp. 544–548.
- [2] C. Atkeson, "Big hero 6: Let's build baymax," *build-baymax.org*, 2015.
- [3] V. Duchaine, N. Lauzier, and C. Gosselin, "On the design of human-safe robot manipulators," *Robot Manipulators New Achievements*, 2010.
- [4] R. J. Kirschner, N. Mansfeld, S. Abdolshah, and S. Haddadin, "Experimental analysis of impact forces in constrained collisions according to ISO/TS 15066," in *2021 IEEE International Conference on Intelligence and Safety for Robotics (ISR)*. IEEE, 2021, pp. 1–5.
- [5] D. Büchler, H. Ott, and J. Peters, "A lightweight robotic arm with pneumatic muscles for robot learning," in *2016 International Conference on Robotics and Automation (ICRA)*, Stockholm, May 2016.
- [6] D. Büchler, R. Calandra, B. Schölkopf, and J. Peters, "Control of Musculoskeletal Systems using Learned Dynamics Models," *IEEE Robotics and Automation Letters*, 2018.
- [7] D. Büchler, S. Guist, R. Calandra, V. Berenz, B. Schölkopf, and J. Peters, "Learning to play table tennis from scratch using muscular robots," *IEEE Transactions on Robotics*, vol. 38, no. 6, pp. 3850–3860, 2022.
- [8] G. B. Avanzini, N. M. Ceriani, A. M. Zanchettin, P. Rocco, and L. Bascetta, "Safety control of industrial robots based on a distributed distance sensor," *IEEE Transactions on Control Systems Technology*, vol. 22, no. 6, pp. 2127–2140, 2014.
- [9] B. Schmidt and L. Wang, "Depth camera based collision avoidance via active robot control," *Journal of Manufacturing Systems*, vol. 33, no. 4, pp. 711–718, 2014.
- [10] P. A. Lasota, G. F. Rossano, and J. A. Shah, "Toward safe close-proximity human-robot interaction with standard industrial robots," in *2014 IEEE International Conference on Automation Science and Engineering (CASE)*. IEEE, 2014, pp. 339–344.
- [11] P. Rybski, P. Anderson-Sprecher, D. Huber, C. Niessl, and R. Simmons, "Sensor fusion for human safety in industrial workcells," in *2012 IEEE/RSJ International Conference on Intelligent Robots and Systems*. IEEE, 2012, pp. 3612–3619.
- [12] M. Heger, "Consideration of risk in reinforcement learning," in *Machine Learning Proceedings 1994*. Elsevier, 1994, pp. 105–111.
- [13] V. S. Borkar, "Q-learning for risk-sensitive control," *Mathematics of Operations Research*, vol. 27, no. 2, pp. 294–311, 2002.
- [14] P. Geibel and F. Wysotzki, "Risk-sensitive reinforcement learning applied to control under constraints," *Journal of Artificial Intelligence Research*, vol. 24, pp. 81–108, 2005.
- [15] A. Basu, T. Bhattacharyya, and V. S. Borkar, "A learning algorithm for risk-sensitive cost," *Mathematics of Operations Research*, vol. 33, no. 4, pp. 880–898, 2008.
- [16] J. Garcia and F. Fernández, "Safe exploration of state and action spaces in reinforcement learning," *Journal of Artificial Intelligence Research*, vol. 45, pp. 515–564, 2012.
- [17] A. Geramifard, J. Redding, and J. P. How, "Intelligent cooperative control architecture: A framework for performance improvement using safe learning," *Journal of Intelligent & Robotic Systems*, vol. 72, pp. 83–103, 2013.
- [18] F. Berkenkamp, M. Turchetta, A. Schoellig, and A. Krause, "Safe model-based reinforcement learning with stability guarantees," *Advances in Neural Information Processing Systems*, vol. 30, 2017.
- [19] Y. Chow, O. Nachum, E. Duenez-Guzman, and M. Ghavamzadeh, "A Lyapunov-based approach to safe reinforcement learning," *Advances in Neural Information Processing Systems*, vol. 31, 2018.
- [20] G. Dalal, K. Dvijotham, M. Vecerik, T. Hester, C. Paduraru, and Y. Tassa, "Safe exploration in continuous action spaces," *arXiv preprint arXiv:1801.08757*, 2018.
- [21] T.-H. Pham, G. De Magistris, and R. Tachibana, "Opt-Layer – Practical constrained optimization for deep reinforcement learning in the real world," in *2018 IEEE International Conference on Robotics and Automation (ICRA)*. IEEE, 2018, pp. 6236–6243.
- [22] Y. S. Shao, C. Chen, S. Kousik, and R. Vasudevan, "Reachability-based trajectory safeguard (RTS): A safe and fast reinforcement learning safety layer for continuous control," *IEEE Robotics and Automation Letters*, vol. 6, no. 2, pp. 3663–3670, 2021.

- [23] J. Garcia and F. Fernández, “A comprehensive survey on safe reinforcement learning,” *Journal of Machine Learning Research*, vol. 16, no. 1, pp. 1437–1480, 2015.
- [24] J.-J. Park, J.-B. Song, and H.-S. Kim, “Safe joint mechanism based on passive compliance for collision safety,” in *Recent Progress in Robotics: Viable Robotic Service to Human: An Edition of the Selected Papers from the 13th International Conference on Advanced Robotics*. Springer, 2008, pp. 49–61.
- [25] J.-J. Park, B.-S. Kim, J.-B. Song, and H.-S. Kim, “Safe link mechanism based on nonlinear stiffness for collision safety,” *Mechanism and Machine Theory*, vol. 43, no. 10, pp. 1332–1348, 2008. [Online]. Available: <https://www.sciencedirect.com/science/article/pii/S0094114X07001577>
- [26] D. V. Gealy, S. McKinley, B. Yi, P. Wu, P. R. Downey, G. Balke, A. Zhao, M. Guo, R. Thomasson, A. Sinclair *et al.*, “Quasi-direct drive for low-cost compliant robotic manipulation,” in *2019 International Conference on Robotics and Automation (ICRA)*. IEEE, 2019, pp. 437–443.
- [27] M. F. Stoelen, F. Bonsignorio, and A. Cangelosi, “Co-exploring actuator antagonism and bio-inspired control in a printable robot arm,” in *International Conference on Simulation of Adaptive Behavior*. Springer, 2016, pp. 244–255.
- [28] M. F. Stoelen, R. de Azambuja, B. L. Rodríguez, F. Bonsignorio, and A. Cangelosi, “The GummiArm project: A replicable and variable-stiffness robot arm for experiments on embodied AI,” *Frontiers in Neurorobotics*, vol. 16, 2022.
- [29] T. Lens, J. Kunz, O. Von Stryk, C. Trommer, and A. Karguth, “BioRob-Arm: A quickly deployable and intrinsically safe, light-weight robot arm for service robotics applications,” in *ISR 2010 (41st International Symposium on Robotics) and ROBOTIK 2010 (6th German Conference on Robotics)*. VDE, 2010, pp. 1–6.
- [30] B. Tondu, S. Ippolito, J. Guiochet, and A. Daidie, “A seven-degrees-of-freedom robot-arm driven by pneumatic artificial muscles for humanoid robots,” *The International Journal of Robotics Research*, vol. 24, no. 4, pp. 257–274, 2005.
- [31] I. Boblan and A. Schulz, “A humanoid muscle robot torso with biologically inspired construction,” in *ISR 2010 (41st International Symposium on Robotics) and ROBOTIK 2010 (6th German Conference on Robotics)*. VDE, 2010, pp. 1–6.
- [32] S. Ikemoto, Y. Nishigori, and K. Hosoda, “Direct teaching method for musculoskeletal robots driven by pneumatic artificial muscles,” in *2012 IEEE International Conference on Robotics and Automation*. IEEE, 2012, pp. 3185–3191.
- [33] S. Ikemoto, F. Kannou, and K. Hosoda, “Humanlike shoulder complex for musculoskeletal robot arms,” in *2012 IEEE/RSJ International Conference on Intelligent Robots and Systems*. IEEE, 2012, pp. 4892–4897.
- [34] D. Gong, R. He, Y. Wang, and J. Yu, “Bionic design of a 7-DOF human-arm-like manipulator actuated by antagonized pneumatic artificial muscles,” in *2019 IEEE 9th Annual International Conference on CYBER Technology in Automation, Control, and Intelligent Systems (CYBER)*. IEEE, 2019, pp. 1503–1508.
- [35] R. Schiavi, A. Bicchi, and F. Flacco, “Integration of active and passive compliance control for safe human-robot coexistence,” in *2009 IEEE International Conference on Robotics and Automation*. IEEE, 2009, pp. 259–264.
- [36] T. Lens, O. von Stryk, and A. Karguth, “Safety properties and collision behavior of robotic arms with elastic tendon actuation,” in *ROBOTIK 2012; 7th German Conference on Robotics*. VDE, 2012, pp. 1–6.
- [37] S. Mori, K. Tanaka, S. Nishikawa, R. Niiyama, and Y. Kuniyoshi, “High-speed and lightweight humanoid robot arm for a skillful badminton robot,” *IEEE Robotics and Automation Letters*, vol. 3, no. 3, pp. 1727–1734, 2018.
- [38] V. Berenz, M. Naveau, F. Widmaier, M. Wüthrich, J.-C. Passy, S. Guist, and D. Büchler, “The o80 C++ templated toolbox: Designing customized python APIs for synchronizing realtime processes,” *Journal of Open Source Software*, vol. 6, no. 66, p. 2752, 2021.
- [39] R. J. Kirschner, A. Kurdas, K. Karacan, P. Junge, S. A. B. Birjandi, N. Mansfeld, S. Abdolshah, and S. Haddadin, “Towards a reference framework for tactile robot performance and safety benchmarking,” in *2021 IEEE/RSJ International Conference on Intelligent Robots and Systems (IROS)*. IEEE, 2021, pp. 4290–4297.
- [40] “ISO/TS 15066. Robots and robotic devices – Collaborative robots.” International Organization for Standardization, Geneva, CH, Technical Specification, Feb. 2016.
- [41] H. Ma, D. Büchler, B. Schölkopf, and M. Muehlebach, “A learning-based iterative control framework for controlling a robot arm with pneumatic artificial muscles,” in *Robotics: Science and Systems*, 2022.
- [42] J. Schulman, F. Wolski, P. Dhariwal, A. Radford, and O. Klimov, “Proximal Policy Optimization Algorithms,” *arXiv:1707.06347 [cs]*, Jul. 2017, arXiv: 1707.06347. [Online]. Available: <http://arxiv.org/abs/1707.06347>